IntechOpen *Journals*

Green Energy and Environmental Technology

RESEARCH PAPER

Nanofibers for Renewable Energy

Michael Wildy and Ping Lu*

Department of Chemistry and Biochemistry, Rowan University, Glassboro, NJ, USA
*Corresponding author. E-mail: lup@rowan.edu

Abstract

Electrospinning is a straightforward technique for the fabrication of nanofibers with the potential for various applications. Thermal energy storage systems using electrospun nanofibers have gained researchers' attention due to its desirable properties such as nanoscale diameter, large surface area, excellent thermal conductivity, and high loading and thermal energy storage capacity. The encapsulation of phase change materials (PCMs) in electrospun nanofibers for storing renewable thermal energy can be achieved by uniaxial electrospinning of a blend of PCM and polymer, coaxial electrospinning of a PCM core and a polymer sheath, or post-electrospinning absorption. The PCM content and thermal energy storage capacity of different PCM composite nanofibers are compared in this chapter. The drawbacks of traditional electrospinning PCM encapsulation techniques and benefits of post-electrospinning encapsulation methods are discussed.

Keywords: nanofibers, renewable energy, latent heat storage, electrospinning, phase change materials, polymers

Citation
Michael Wildy and Ping Lu (2022), Nanofibers for Renewable Energy. *Green Energy and Environmental Technology* 2022(0), 1–25.

DOI
https://doi.org/10.5772/geet.03

Published
28 March 2022

1. Introduction

1.1. Fabrication of nanofibers

Nanofibers are defined as fibers with diameters <100 nm, or in the context of textiles, <1000 nm. A primary property of nanofibers is high specific surface area due to their extremely small diameter and large percent of molecules at the surface [1]. Electrospinning is a facile method for the fabrication of nonwoven and continuous polymer fibers with diameters in the nanometer scale to several micrometer scale. The process involves a polymer solution or a polymer melt in a syringe that is forced through a needle by a syringe pump at a desired feed rate. A conductive metal collector, either a flat or rotating drum, is positioned at some distance away from the needle while high-voltage current is supplied to the spinneret (needle). Columbic forces in the charged solution cause the droplet at the spinneret to elongate into a Taylor cone [2]. Jets eject and accelerate from the tip of the Taylor cone, elongate and coil as they reach the collector as a result of repulsive forces from the charges in the fluid jet, causing instability and pulling towards the

conductive collector. After rapid evaporation of solvents and solidification of the thin jets, polymer fibers are deposited on the collector (2). Uniaxial electrospinning is the simplest, where a single polymer solution is used. Coaxial electrospinning is more complex and combines multiple polymer solutions to create core-sheath composite nanofibers. Electrospinnable materials include polymers such as polyethylene (PE), polypropylene (PP), polystyrene (PS), poly(methyl methacrylate) (PMMA), polyacrylonitrile (PAN), polyamide 6 (PA6), poly(ethylene terephthalate) (PET), poly(vinyl chloride) (PVC), poly(vinyl alcohol) (PVA), polylactide (PLA), polyvinylpyrrolidone (PVP), poly(vinyl butyral) (PVB), gelatin, cellulose, etc. [3], and organic/inorganic composites such as PVP/Al_2O_3, PVB/Al_2O_3, and PA6/ZnO [4, 5]. Many factors can influence the properties of electrospun nanofibers, such as the polymer and solvent system, concentration, feed rate, temperature, relative humidity, voltage, needle diameter, and tip-collector distance, etc [6]. Electrospun nanofibers have been used in a variety of applications including catalysis, sensors, filtration, energy storage, tissue engineering, and drug delivery, among other things [7–10].

1.2. Phase change materials

The forms of thermal energy include sensible heat (e.g., from temperature change), latent heat (e.g., from phase change), and chemical heat (e.g., from a chemical reaction). Phase change materials (PCMs) utilize latent heat and possess higher energy density than sensible heat and are less expensive than chemical heat. Latent heat of fusion is absorbed or released by PCMs during the freezing or melting processes [11]. The high enthalpy of fusion of PCMs as well as their relatively small change in volume makes solid–liquid PCMs particularly attractive as thermal energy storage materials. Solid–liquid PCMs can improve thermal management of energy storage by increasing efficiency of storage and use [12]. PCMs also have the advantage of high energy storage density at almost isothermal conditions and a small temperature change between cycles of energy retrieval and storage [13]. Another practical advantage of PCMs is that their narrow ranges of upper and lower phase transition temperatures can meet the requirements of the working range for desired applications.

PCMs can be classified as either organic or inorganic. Inorganic PCMs include salt hydrates and metallics. Metals and metal alloys with low melting temperatures are usually not considered practical PCMs due to their weight limitations. The disadvantages of salt hydrates are their instability and degradation when heated, water loss after each heating cycle, incongruent melting, and supercooling [14, 15]. Organic PCMs include paraffin waxes, poly(ethylene glycol)s (PEGs), alcohols, fatty acids, and their derivatives and eutectics [16, 17]. Paraffin waxes are one of the most commonly used PCMs due to their high latent heat, good stability, and low

corrosivity and cost [18]. Octadecane is a paraffin based PCM with a melting temperature close to that of the human body and has potential as a PCM to be used in the textile industry. Advantages of organic PCMs include high latent heat of fusion, nontoxicity, non-corrosivity, low supercooling, no phase separation upon heating/cooling cycles [15]. Fatty acids commonly used as PCMs are stearic, lauric, myristic, capric, palmitic, and caprylic acids [17]. Fatty acids have high heats of fusion, comparable to paraffin waxes, and reproducible melting/freezing cycles with minimal supercooling [15]. The most notable disadvantages of organic PCMs are their low thermal conductivity, which can suppress the thermal energy storage capabilities of PCMs and result in containment issues. Biobased PCMs are a newer type of organic PCMs and are derived from sources like plant oils and beef tallow. Biobased PCMs have high latent heat, low flammability, and good thermal stability as a result of being fully hydrogenated [17]. Many PCMs have been incorporated into electrospun nanofibers, including paraffin waxes [19], biobased PCMs [20–22], PEGs [23–27], fatty acids and eutectics [28–33] as well as others [18].

1.3. Thermal energy storage systems

The proper containment of PCMs inside a thermal energy storage system is a major challenge. Leakage of PCMs from the system can not only result in diminishing efficiency and short lifespan, but also cause severe environment pollution issues. A typical thermal energy storage (TES) system is composed of a PCM and a framework/supporting material, in which the PCM is either encapsulated or incorporated into a form-stable material. Both organic and inorganic frameworks/supporting materials have been used for TES systems. PCMs for TES systems are usually in the form of macro-, micro-, or nano-capsules [34] consisting of a wide range of organic and inorganic materials, such as n-octadecane (C18) in a titania shell [35], paraffin in low-density polyethylene-ethylvinylacetate (LDPE-EVA) [36], and stearic acid (SA) in SiO_2 [37]. These core-shell capsules typically have PCM loadings near 50%–60% [38], but higher PCM loadings, up to 80%, has also been reported [35]. However, the overall loading capacity can be further reduced when these PCM-containing capsules are incorporated into bulk supporting materials such as foams, films, and fibers [39–42].

Creating a TES system with the smallest possible size is important to allow for almost instantaneous freezing and melting of PCMs [43]. Various TES systems made of composite nanofibers have been developed by researchers. Uniaxial electrospinning of a blend of PCM and polymer is a simple way to fabricate nanofiber based TES systems, which has been used to fabricate TES systems containing PS [28, 44], PLA [45], PA6 [27], PAN [46] and PET [33] as the support materials. Coaxial electrospinning of a PCM as the core and a polymer as the sheath has also been reported, in which TiO_2-polyvinylpyrrolidone (PVP) [47],

polyurethane (PU) [22, 48, 49], polyvinylidene fluoride (PVDF) [50], polyvinyl butyral (PVB) [51], and cellulose acetate (CA) [23, 52] and other polymers were used as sheath materials [18].

2. Encapsulation of PCMs into nanofibers

Nanofibers are advantageous for encapsulating PCMs and forming structure-stable TES systems as they possess very small diameters and high specific surface areas. The encapsulation of PCMs in nanofibers can be accomplished by either electrospinning the PCMs and polymers concurrently or incorporating PCMs into nanofibers after electrospinning. These different methods are compared in the following sections.

2.1. In-situ encapsulation

2.1.1. Blend electrospinning

Blend electrospinning involves the mixing the PCMs into the polymer solution prior to uniaxial electrospinning. The dissolution or dispersion of compounds into the solution depends on the solution's physicochemical properties and intermolecular interactions [53]. Factors that most affect the solution electrospinnability and nanofiber properties are the solvent system and mass ratio of components (PCMs and polymers) [18]. Emulsions are sometimes created to blend polymers and PCMs that are not both soluble in the same solvent system. Zdraveva *et al.* prepared an oil/water emulsion of a mixture of plant oil PCM and sodium dodecyl sulfate (SDS) before blending with poly(vinyl alcohol) (PVA) aqueous solutions. The PCM composite nanofibers had a maximum PCM content of 70% of polymer by weight. Adding more than 70% PCM caused the separation of PCM from solution and impacted the PCM distribution in nanofibers [21]. Kizildag reported the fabrication of smooth and uniform paraffin wax/PAN composite nanofibers by blend electrospinning with maximum PCM content of 50% of polymer [54]. Unfortunately, it is difficult to completely encapsulate PCMs inside nanofibers using uniaxial electrospinning because of the tendency for some of the PCM to distribute on the nanofiber surface [18]. Lu *et al.* reported no measurable PCM leakage in blend electrospun LA/PS nanofibers. This can be attributed to a good compatibility between LA and PS as well as the superior mechanical strength of PS. The LAPS composite nanofibers were fabricated by uniaxial electrospinning a blend solution. The LA/PS solution weight ratios were 1/4, 1/2, 1/1, 2/1, 3/1, and 4/1, and the composite nanofibers were named $LA_{0.25}$ *PS*, $LA_{0.5}$ *PS*, LA_1 *PS*, LA_2 *PS*, LA_3 *PS*, and LA_4 *PS*, respectively. Surface porosity was not observed in the LA/PS composite nanofibers and their surface roughness increased with increasing LA content, most likely resulting from phase separation. It was noted that electrospinning behavior and phase separation was affected by the introduction of PCM. The vapor induced phase separation observed under the identical conditions with pure PS

electrospinning [55] was inhibited by the addition of only a small amount of LA. Due to the hydrophilic nature of LA, atmospheric water vapor was not able to induce phase separation and form pores inside the composite nanofibers [28].

Additionally, uniaxial blend electrospinning can induce phase separation between PCM and polymer matrix, leading to the formation of PCM rich and polymer rich domains inside and on the surface of nanofibers. Domain size is an important factor in the crystallization and supercooling processes. It was reported that small PCM domain sizes could decrease the number of nuclei in a melt. This can result in an increase of supercooling effect and broadening of temperature range of phase change [56]. Furthermore, the distribution of some of the PCM domains onto or near the surface of the nanofibers further broadens the temperature range of phase change and leads to potential leakage. This is due to the phenomenon of small particles having a lower melting temperature than the same bulk material. Thus, the smaller surface PCM domains will melt before the main internal PCM domains [43]. Accordingly, the distribution and aggregation of PCMs need to be optimized in blend electrospinning method for fabricating TES systems. It was also reported that the formation of deformed or nonuniform fibers can occur when the PCM content is too high [57]. Therefore, depending on the interaction between the PCM and the supporting material, PCM loading capacity in blend electrospun nanofibers can vary greatly.

2.1.2. *Coaxial electrospinning*

Coaxial electrospinning allows for the fabrication of continuous core-sheath nanofibers from two solutions using two nozzles concentrically aligned in a single spinneret. The core and sheath solutions are fed at individually controlled feed rates through the inner and outer nozzles, respectively. The core-sheath structure completely encapsulates the PCMs in the fibers without leakage when electrospinning parameters are optimized. Additional parameters need to be optimized for coaxial electrospinning because two solutions are used [58]. If the feed rate of the core solution is too high, the core solution will mix with the sheath to disrupt the separation of the two layers [59]. Coaxial electrospinning has been employed for the encapsulation of PCMs using hydrophilic and hydrophobic polymers as the sheath materials. Sun *et al.* reported electrospinning octadecane PCM core with hydrophobic polyvinyl butyral (PVB) sheath using nontoxic ethanol as the solvent. The octadecane/PVB core-sheath nanofibers had a maximum PCM content of 46.4% [51]. Coaxial electrospinning was also reported to be used to fabricate core-sheath nanofibers of bio-based PCM, natural soy wax, and PU. The core solution PCM concentration was increased from 10% to 60%. In nanofibers with PCM concentrations of 40% and greater, beads were observed on the surface and found to fuse together and solidify into randomly dispersed structures on the membrane [48]. Rezaei *et al.* and Chen *et al.* fabricated coaxial electrospun

nanofibers containing a PEG core inside a CA sheath. The PEG/CA nanofibers had maximum PCM mass contents of 34.5% and 43.2%, respectively [23, 25]. Lu *et al.* produced paraffin wax core and PAN sheath nanofibers with 54.3% PCM encapsulation efficiency via coaxial electrospinning [60]. While coaxial electrospinning of PCM composite nanofibers has the disadvantage of increased complexity due to added parameters to optimize, this electrospinning technique can alleviate PCM containment concerns that arise from random distribution of PCMs in blend nanofibers using uniaxial electrospinning. Additional combinations of different PCMs and polymers are also possible since it is not necessary to use the same solvent for both the core and sheath layers. Usually, the sheath polymer should not be miscible with the core solvent to ensure proper separation of layers and complete encapsulation of PCMs. Unfortunately, the loading capacity of PCM in composite nanofibers prepared by the coaxial electrospinning technique is usually much lower than composite nanofibers by the uniaxial electrospinning technique. Additionally, instability of electrospinning resulting from the incompatibility of PCMs, polymers and solvents can severely interfere with the production of uniform PCM composite nanofibers [18].

2.2. Post electrospinning PCM incorporation

2.2.1. Thermally triggered encapsulation

Thermally triggered encapsulation is accomplished by allowing a supporting material to be in contact with molten PCMs for a sufficient amount of time to allow the diffusion of PCMs into the material. This encapsulation method was used for the incorporation of fatty acid eutectics PCMs in bulk materials. Yang *et al.* encapsulated ternary eutectic mixture of myristic–palmitic–stearic acid (MA–PA–SA) in expanded graphite (EG). EG was placed in beakers with fatty acid, sealed, and heated at 65 °C for 24 h in an oven [61]. Zhang *et al.* encapsulated LA–MA–PA ternary eutectic into EG by a similar method. The fatty acid eutectics and EG were placed in beakers and heated at 50 °C for 20 h. This method allowed for the absorption of the liquid fatty acid eutectics into the porous EG structure uniformly [62].

In nanofibers, encapsulation is facilitated by capillary and intermolecular forces to allow fluid traveling through internal pores. This is similar to the explanation of the rise of sap in trees relying on the cohesion-tension (CT) theory [63]. Lu *et al.* developed a method for thermally triggered encapsulation of PCM into porous electrospun PS nanofibers using lauric acid (LA) as the PCM. This method allowed for the encapsulation of LA inside the internal pores of PS with the aid of capillary forces and intermolecular forces. Figure 1 depicts the process of sap rise in trees and capillary diffusion and the thermally triggered encapsulation of molten LA in the PS nanofiber membrane. PS nanofibers with internal porosity was fabricated by

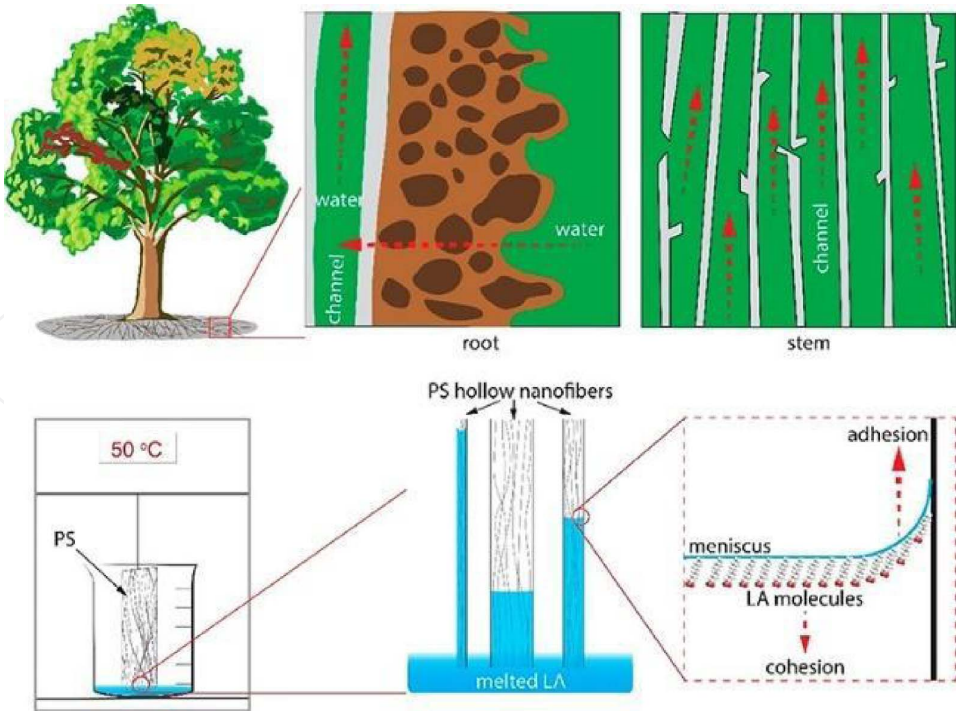

Figure 1. Illustrated schematics of the diffusion of water (or sap) through channels in a tree (top) and thermally triggered encapsulation by diffusion of molten LA into PS nanofibers (bottom) [29].

electrospinning a 20 wt% solution of PS in DMF at 20 °C and 45% relative humidity. The collector used was a piece of aluminum foil wrapped around a rotating drum. Since the drum was rotating at a sufficiently high speed, the majority of the nanofibers were deposited along the direction of rotation. LA was melted at 50, 60, 70, and 80 °C ($LAPS_{50}$, $LAPS_{60}$, $LAPS_{70}$, and $LAPS_{80}$) in an oven and PS nanofiber membranes (9 cm × 4 cm × 0.2 cm) were in contract with the surface of the liquid LA for 24 h, an adequate time to reach equilibrium. The LA loaded PS membrane was allowed to dry at room temperature in a fume hood. The diffusion rate of the melted LA in the PS nanofibers was found to be ~0.375 cm/h at 60 °C. Since the LA diffused through the nanochannels of the PS nanofibers, the interfiber spacing was left void. Furthermore, no leakage of LA to the surface of the nanofibers was observed. The temperature of the heated PCM had an important impact on the diffusion of LA through the PS nanofibers. It was found that LA stopped diffusing up into the membrane at temperatures above 70 °C, even if left for an extended period of time. While the temperature of LA had little effect on the cohesion of LA, the adhesion of LA and PS was negatively impacted because of increased kinetic energy of LA molecules at higher temperatures. The distribution of LA was investigated by TGA and found to be uniform throughout the composite nanofiber membrane [29].

Lu *et al.* studied the factors that influenced the formation of porous PS nanofibers. DMF was used as the solvent in the fabrication of PS nanofibers [28–30]. Since DMF has a lower vapor pressure than water, it was assumed that water saturated the air jet interface and penetrated the jet to act as a nonsolvent at the relative humidity of 42% and 62%, and cause some of the PS to precipitate to the surface of the fibers, forming a sheath layer. This sheath layer further slowed the evaporation rate of DMF and water, allowing for phase separation and the formation of internal pores. Further, PS possesses great mechanical strength and insulating properties to improve the overall performance of the TES systems [55].

Cai *et al.* reported the fabrication of TES systems composed of electrospun SiO_2 nanofiber mats as supporting materials for fatty acid eutectics using a similar method [64]. The nanofibers were pyrolyzed prior to encapsulation of the PCMs. Capric–lauric–palmitic acid (CA–LA–PA) eutectic mixture was placed in beakers and melted at 60 °C and SiO_2 nanofiber mat was fully immersed for 12 h to reach saturated absorption and hung in an oven at 60 °C for 10 h to remove residual FA eutectic mixture. In contrast to the internal encapsulation of the PCMs in the porous PS nanofibers, fatty acid eutectics were encapsulated in and supported by the nanofiber membrane through physical absorption. This method used the interfiber porosity of the nonwoven nanofiber membrane to make a nanofiber/PCM composite mats as the form-stable PCM composites instead of the intrafiber porosity to create form-stable PCM nanofibers. Cai *et al.* also fabricated form-stable PCM composite nanofibrous mats of fatty acid eutectics and PA6 nanofibers. A piece of PA6 nanofiber mat (5 cm × 5 cm) was immersed in fatty acid eutectics at 60 °C for 10 h to reach saturation equilibrium and then hung in an oven at 60 °C for 10 h to remove residual fatty acid eutectics [32]. In both cases [32, 64], the PCMs were present in the interfiber spacings of the nanofiber mat as well as in the intrafiber pores of nanofibers. Due to strong capillary and surface tension forces, no PCM leakages from the nanofiber mats were noticed. However, form-stable PCM composite nanofibers containing PCMs in intrafiber pores are more desirable than PCMs in interfiber pores because of their enhanced thermal stability and practicality [18].

2.2.2. *Solvent-assisted encapsulation*

Building on their previous work [29], Lu *et al.* developed an improved encapsulation technique with the addition of solvent to the PCM. Solvent-assisted encapsulation is very similar to thermal encapsulation, except the PCM is dissolved in a solvent prior to partially immersing the supporting material. As in the case in thermal encapsulation, capillary forces are also responsible for the diffusion of PCM solution through the nanochannels in polymer nanofibers. A piece of polystyrene nanofiber mat (12 cm × 3 cm × 0.2 cm) was in contact with the liquid interface of a 10 ml solutions of 0.01–0.6 g/ml in capped glass bottles at room temperature until reaching equilibrium in 1 h. The LAPS composite nanofibers were then hung to dry at room

temperature in a fume hood. The diffusion of LA ethanol solution reached the top edge of the fiber mat within 30 min. The 0.1 g/ml LA ethanol solution had a diffusion rate of ~24 cm/h, about 64 times greater than diffusion rate of melted LA in PS nanofibers [29]. This technique was also successful in encapsulating the LA internally while leaving the interfiber spacing and surface of the PS nanofibers free of PCM. The LA content was measured in different portions of the membrane and the LA distribution was found to be homogenous and uniform. PCM loading was controlled by solution concentration. Solutions of LA in ethanol with concentrations of 0.01, 0.05, 0.1, 0.2, 0.4, and 0.6 g LA/ml ethanol were compared to study the effect of initial solution concentration on PCM loading. It was found that the LA loading inside the PS nanofibers was increased with increasing the initial LA concentration, except in the case of 0.6 g/ml. All solution concentrations resulted in the encapsulation of LA internally, with surfaces free of any LA [30].

3. Thermal energy storage performance

Thermal energy storage and TES system performance are influenced by the loading capacity and overall content of PCMs in nanofibers. These properties are investigated by studying their thermo-physical properties after repeated thermal cycles and the structure/morphology of PCM composite nanofibers.

3.1. PCM content and distribution in nanofibers

The content and distribution of PCMs in TES systems play an important role in the thermal energy storage capacity and performance. The thermal energy storage capacity is a function of PCM content and other TES system properties. Latent heat of fusion is used as a measure of thermal energy storage capacity. The specific latent heat absorbed or released by a PCM composite material should be as close as possible to that of the pristine PCM. A common technique to measure melting temperature and heat of fusion is differential scanning calorimetry (DSC). DSC is a thermo-analytical technique that measures the difference in heat needed to change the temperature of sample and the reference material as a function of temperature. The recommended reference material for PCMs is alumina (Al_2O_3) since it has a well-defined heat capacity over the scanned temperature range. During a phase change, the sample requires either more heat if it is exothermic (i.e., melting) or less heat if it is endothermic (i.e., exothermic) processes. DSC measures the difference in heat between the reference and sample to calculate the amount of heat absorbed or released by the sample during the temperature change and/or phase change. The DSC scans are overlaid and plotted as the DSC curve. The phase transition temperature range is between the phase transition temperature (i.e., melting or crystallization temperature), found as the onset of the line fitting of the rising portion of the peak, and the temperature corresponding to the peak. Latent heat of

fusion is calculated as the area under the curve during the heating/melting process [65]. Several calculation methods are used to determine the content of PCMs in nanofibers. The simplest method of calculating the PCM content in nanofibers is to use the mass ratios of the PCMs and polymers for blend electrospinning. The theoretical PCM content can also be calculated using the PCM and polymer concentrations and feed rates of the solutions for coaxial electrospinning. An alternative method is to selectively remove the PCM by a solvent and the weight loss can be used to estimate the PCM content. The most accurate method is to measure the PCM weight loss during the thermal decomposition of PCM composite nanofibers by thermogravimetric analysis (TGA). A similarly accurate method is to use the enthalpies to calculate the encapsulation ratio of PCM by DSC. In some cases where the PCM is absorbed into the nanofiber membrane, the absorption capacity is used to determine the PCM content.

The PCM contents and enthalpies of composite nanofibers made from blend electrospinning, thermally triggered encapsulation, and solvent assisted encapsulation were measured by simultaneous TGA-DSC technique. TGA measures the change in weight (or mass) as a function of temperature while DSC can identify glass transition temperature, melting and crystallization temperatures, and cross-linking. Additionally, DSC is normalized for the instantaneous weight instead of relying on the initial weight. The TGA thermogram of pure PS nanofibers showed a degradation and nearly 100% weight loss in one step between 350–450 °C. The pure LA thermogram showed a degradation and 97.8% weight loss in one step between 100–300 °C. The thermograms of LAPS composite nanofibers displayed two step decomposition at 100–300 °C and 350–450 °C corresponding to LA and PS decompositions, respectively. The weight loss in the 100–300 °C temperature range was used to estimate the percentage of LA in the composite nanofibers. In blend electrospun LAPS nanofibers, weight losses corresponding to LA content were 16.6%, 30.6%, 47.2%, 65.7%, 73.6%, and 78.4% for $LA_{0.25}$ *PS*, $LA_{0.5}$ *PS*, LA_1 *PS*, LA_2 *PS*, LA_3 *PS*, and LA_4 *PS*, respectively. These weight losses matched the weight ratios of LA in the blend solutions and confirmed uniform distribution of LA in nanofibers. Increase of LA content resulted in weakening of the peak at 416 °C, corresponding to the endothermic decomposition of PS, confirming decreasing PS content. The melting peak of LA strengthened and shifted to a slightly higher temperature, likely caused by peak broadening effect. Furthermore, the decomposition signal of LA was not strong enough to distinguish in $LA_{0.25}$ *PS* and $LA_{0.5}$ *PS* but was observed in $LA_{1.0}$ *PS* and increased in strength and shifted slightly to a higher temperature with increasing LA content [28].

The thermal energy storage capacity of blend electrospun LAPS composite nanofibers was examined over the temperature range of 0–80 °C for the determination of LA content and thermal energy storage capacity. The heat flow in

DSC analysis was calibrated to give a more accurate temperature than traditional T1 mode which uses the programmed sample temperature instead of the actual temperature. The DSC thermogram of pristine LA showed a unimodal endothermic peak at 44.9 °C, assigned to the melting temperature of LA (t_m). The temperature of melting onset (t_{mo}), 43.7 °C, was higher than the temperature of crystallization (t_{oc}), 40.0 °C. This phenomenon can be explained by the supercooling effect. Crystallization processes typically involve two steps: the formation of nuclei and crystal growth. Crystallization can occur when a material is cooled to a temperature where the free enthalpy of the crystal becomes smaller than the free enthalpy of melt and enough nuclei are present. If a sufficient number of nuclei are not present, it is possible for a material to be cooled beyond its freezing point without solidifying. Supercooling is undesirable since it lowers and broadens the temperature range of latent heat release. During the crystallization phase transition, exothermic latent heat is generated. This caused the temperature to rise to 42.9 °C, forming an irregular peak not observed in T1 mode. The crystallization of $LA_{0.25}PS$ occurred over a wide temperature range of 39.2–21.1 °C. This was caused by the partial isolation of the small LA domains by the large PS matrix, leading to fewer nuclei and supercooling [56]. A bimodal melting peak was observed for nanofibers with lower concentrations of LA, attributed to the small portion of LA distributed on or near the surface and these small LA domains on the supporting surface had lower melting temperature than the large LA domains inside nanofibers [43]. The supercooling effect was weakened by increasing LA content and the formation of larger LA domains. The enthalpy of melting of the LAPS nanofibers increased from 6.8 J/g for $LA_{0.25}PS$ to 141.3 J/g for LA_4PS. The enthalpy of melting of LA is 180.2 J/g and the maximum storage capacity was 78.4% and observed in LA_4PS [28].

The weight loss and corresponding LA content in LAPS nanofibers prepared by thermally triggered encapsulation were greater than those fabricated by blend electrospinning technique. LA contents were 81.5%, 51.5%, 6.1%, and 3.5%, for $LAPS_{50}$, $LAPS_{60}$, $LAPS_{70}$, and $LAPS_{80}$, respectively. The LA content fell to 3.5% when temperature was increased to 80 °C. This was likely caused by a change in interaction between LA and PS, leading to inability of LA from travelling up capillaries at temperatures above 70 °C. Four different sections of the nanofiber mat were analyzed for PCM distribution. A slight gradient of ±1.8% of PCM loading was found, indicating the distribution of LA was homogeneous. The portion of the nanofiber mat that was immersed in LA had 91.1% LA loading. However, LA filled the interfiber spacing, which was able to leak as drips or wetting of objects that were in contact. The thermal energy storage capacity of LAPS nanofibers prepared at 50 °C and 60 °C was analyzed by DSC-TGA. An endothermic peak between 42.4–53.4 °C was observed in the thermogram during heating. A second endothermic smaller peak appeared at 40.6 °C in the thermogram of the $LAPS_{50}$. Similar to the bimodal peak observed in the thermogram of LAPS composite nanofibers made from

uniaxial blend electrospinning, the second peak was attributed to the distribution of a small amount of LA close to the surface which had a lower melting temperature. This bimodal peak gradually disappeared after several thermal cycles, probably due to the consolidation of LA after repeated melting. The supercooling effect was observed in both LAPS nanofibers, with temperatures of crystallization of 42.2 °C and 41.4 °C for $LAPS_{50}$ and $LAPS_{60}$, respectively, which were lower than the temperature of melting onset of LA at 42.4 °C. An irregular crystallization peak was also observed. The maximum enthalpy of melting was 147.1 J/g, corresponding to a maximum of 81.6% thermal energy storage capacity for $LAPS_{50}$ [29].

Solvent-assisted encapsulated LAPS nanofibers exhibited the highest LA loading with weight losses and corresponding LA contents of 10.6%, 36.2%, 50.9%, 71.3%, 82.2%, and 66.1% for LAPS prepared with 0.01, 0.05, 0.1, 0.2, 0.4, and 0.6 g/ml LA ethanol solutions, respectively. The highest LA content resulted from encapsulation with the 0.4 g/ml LA ethanol solution. This result agrees with the SEM observations of dense packing of the 0.4 g/ml compared to the 0.6 g/ml LA ethanol solution encapsulated LAPS nanofibers. Slower diffusion and weakened intermolecular attractions between the solute, solvent, and polymer was likely the reason for the decrease in LA content. The DSC thermogram showed an endothermic peak at 45.4 °C as well as a second weak peak at 41.7 °C were observed in the thermogram during heating, corresponding to the melting of LA and the small domains of LA, respectively. The second peak gradually disappeared after repeated thermal cycles due to the aggregation of small LA domains. Supercooling effect resulted in a crystallization temperature lower than that of LA. An irregular crystallization peak was caused by the release of latent heat since the DCS was not operating in T1 mode. The average enthalpy of melting was found to be 147.8 J/g, corresponding to 82.0% storage capacity with respect to pure LA [30].

In comparison, the content of FA eutectics in high-temperature annealed SiO_2 nanofibers was estimated using equation (1), below, where m_0 is the initial mass and m is the mass after absorption.

$$\text{absorption capacity} = \frac{m - m_0}{m_0} \times 100\%. \quad (1)$$

The calculated absorption capacities were 79.1%, 81.3%, and 79.5% for CA–LA–PA/SiO_2 composite nanofibers prepared from SiO_2 nanofibers annealed at 500 °C, 600 °C, and 700 °C, respectively. The maximum enthalpy of melting was 100.9 J/g, while that of CA–LA–PA was 120.2 J/g [64]. The CA and CA-series fatty acid eutectic content in PA6 nanofiber membranes was also estimated using equation (1). The calculated absorption capacities were 72.7%, 81.9%, 78.0%, and 75.4% for CA–LA, CA–PA, CA–SA, and CA composite nanofiber membranes, respectively. CA-SA/PA6 composite nanofibers had the highest enthalpy of melting

for the different FA eutectics at 116.9 J/g, while that of the respective FA eutectic was 156.8 J/g [32].

Core-sheath composite nanofibers prepared by coaxial electrospinning generally have a lower PCM content than those by blend electrospinning. The PCM content is calculated using enthalpies by equation (2).

$$\text{encapsulation ratio} = \frac{\Delta H_{m,PCM/polymer}}{\Delta H_{m,PCM}} \times 100\%. \quad (2)$$

A maximum encapsulation ratio of octadecane in PVB was found to be 46.4%, using equation (2). The TGA thermogram showed mass loss during heating from 30–300 °C, corresponding to octadecane decomposition, of roughly the same weight percent. The thermal energy storage capacity and the maximum enthalpy of melting of composite nanofibers was found to be 105.9 J/g, while that of pure octadecane was 228.2 J/g [51]. Coaxial electrospun composite nanofibers with paraffin wax in the core and PAN sheath was analyzed by DCS for thermal energy storage capacity and found to have an enthalpy of melting of 60.31 J/g. The corresponding encapsulation efficiency of 54.3% was slightly higher than those mentioned previously [60]. The PEG content in coaxial electrospun nanofibers with CA sheath was calculated using the weights of the nanofibers before and after the removal of PEG in water. The maximum PEG content was found to be 43.2%. The thermal energy storage capacity of the nanofibers was analyzed by DSC. The increase of PEG content had no effect on the phase change temperatures but resulted in an increase in enthalpies. Enthalpies of melting of the composite nanofibers were found to be 53.0 J/g and 60.6 J/g, while that of pure PEG was 177.4 J/g. These results corresponded to a maximum thermal energy storage capacity of 34.2% [25].

Some groups reported PCM content based on the mass percentage of PCM in the electrospinning solution [49, 54]. This oversimplifies the final content of PCM in composite nanofibers, especially when an additional polymer shell is used to encapsulate the PCM core. Uniaxial blend electrospun nanofibers have a relatively large PCM content and is often calculated from the mass ratio of PCM/polymer. The maximum PCM content for blend electrospun mixture of plant waxes and PVA without forming PCM particle clusters was 70%. The TGA thermogram showed a slope corresponding to the PCM decomposition accounting for roughly 45%. This demonstrates the discrepancy between calculated and actual PCM contents. The thermal energy storage capacity of the composite nanofibers was investigated by DSC. The maximum enthalpy of melting of composite nanofibers was found to be 84.72 J/g, while that of the pristine PCM mixture was 221.2 J/g. These results corresponded to a thermal energy storage capacity of 38.3% [21]. The uniaxial blend electrospun LAPA6 composite nanofibers fabricated by Cai *et al.* were investigated for thermal energy storage capacity by DSC. The maximum enthalpy of melting was

74.12 J/g, while that of pure LA was 173.25 J/g. One hour ethanol wash of the LAPA6 nanofibers was used to further examine the distribution of LA. Pores on the surface of the nanofibers were observed by SEM. This indicated that small domains of LA were present on or near the surface. However, after heat treatment at 60 °C and an ethanol wash, the surface pores were not present. Therefore, the heat treatment aided in the encapsulation of LA in the nanofibers [66].

3.2. Physical morphology and size

The physical morphology of nanofibers is commonly analyzed using scanning electron microscopy (SEM) imaging. Gold plasma sputter coating is used to impart conductivity to electrospun nanofibers made of nonconducting material(s). The images provide representations of the nanoscale morphology of the surface and cross-section. Fiber size can be measured by processing software such as ImageJ and the average diameter is typically determined by measuring tens of fibers if not more. Additionally, the internal morphology can be observed after appropriate sample preparation to expose the cross-sectional area of nanofibers [6]. SEM imaging is also useful for analyzing the distribution of PCMs and identifying leakages.

The blend of electrospun LAPS composite nanofibers were examined by SEM. A continuous flat collector was used so the nanofibers were deposited in a randomly oriented mat. The PS and LAPS nanofibers all displayed uniform cylindrical shape and size without bead formations or irregularities. The smoothest surface was observed in the pure PS nanofibers. Surface roughness increased with increase of LA content, most likely as a result of phase separation between LA and PS. The surfaces of the nanofibers were all lacking any notable porosity. The size of nanofibers decreased with the initial introduction of LA. Pure PS nanofibers were the largest, with an average diameter of 1.93 μm. The LA composite nanofibers showed a decrease of ~50% to 0.95 μm in average diameter and a narrower size distribution range after 20% LA was incorporated. The incorporation of 50% LA in nanofibers resulted in the smallest size with an average diameter of 0.78 μm. The introduction of LA in the electrospinning solution affected the electrospinning process and phase separation of the PS nanofibers. The typical internal porosity observed in pure PS nanofibers fabricated at high relative humidity levels resulted from vapor induced phase separation of the hydrophobic PS and environment water vapor [55]. The size of the LAPS composite nanofiber diameter decreased as a result of the addition of LA to the blend solution. This was caused by the LA interfering with the phase separation process that typically occurs with the interaction of atmospheric water vapor and PS in DMF. The trend then changed to increasing diameter with increasing LA content when over 50% LA was incorporated, as a result of increasing amounts of LA being encapsulated. The average diameters of nanofibers were 0.87, 0.98, and 1.30 μm for LA_2 *PS*, LA_3 *PS*, and LA_4 *PS* nanofibers, respectively.

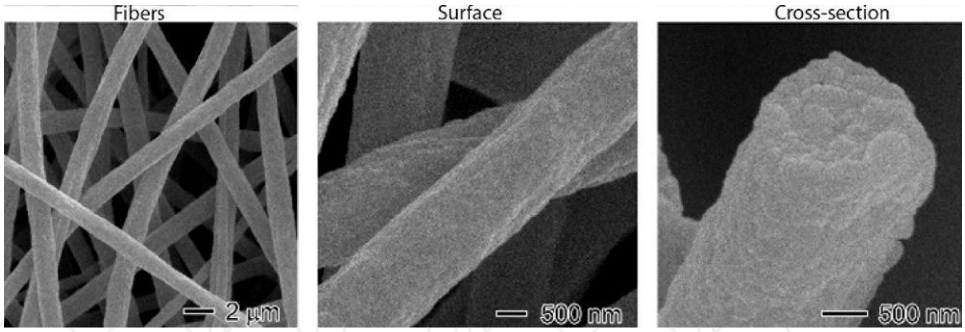

Figure 2. SEM images the overview, surface, and cross-section of LA_4 *PS* nanofibers fabricated by uniaxial blend electrospinning [28].

The porous PS nanofibers were replaced by solid interior, as seen in the cross-sections of LAPS composite nanofibers in figure 2. The cross-section also displayed grainer texture, suggesting the formation of LA rich domains and confirming the successful encapsulation of LA [28].

The thermally triggered encapsulation of LA in PS nanofibers resulted in a slight increase in the average diameter, from 2.27 ± 0.26 μm for pure PS nanofibers to 2.56 ± 0.30 μm, 2.08 ± 0.44 μm, 2.35 ± 0.38 μm, and 2.32 ± 0.32 μm for LA encapsulation at 50, 60, 70, and 80 °C, respectively. SEM images of the surface and cross-section of LAPS nanofibers encapsulated with LA at 50 °C are shown in figure 3. The pure PS nanofibers displayed uniform shape and size without bead formation or irregularities. The relatively negligible effect of thermally triggered LA incorporation on the size of composite nanofibers in comparison to the blend electrospinning method demonstrated the mechanical strength of the PS nanofibers [29]. The solvent assisted encapsulation of LA in PS nanofibers using 0.4 g/ml LA ethanol solution also produced LAPS composite nanofibers with slightly larger diameter. The LAPS nanofibers had an average diameter of 2.45 ± 0.76 μm as opposed to 2.16 ± 0.22 μm in pure PS nanofibers. The LAPS nanofibers also displayed uniform shape and size without bead formation, irregularities, and a smooth surface without any notable pores. A cross-section SEM image, seen in figure 4, shows the interior structure of LAPS nanofibers filled with LA. Some of the internal pores were retained in the LAPS composite nanofibers, suggesting only partially filled nanofibers [30].

SEM images showed PA6 and of SiO_2 nanofibers had uniform size, cylindrical shape, and smooth surface, respectively. The SEM images of the nanofiber mats after absorption of FA eutectics displaced expanded nanofibers with increased diameters. The porous structure of the interfiber spacing of the nanofiber mat provided additional loading capacity by supporting the FA eutectics through capillary and

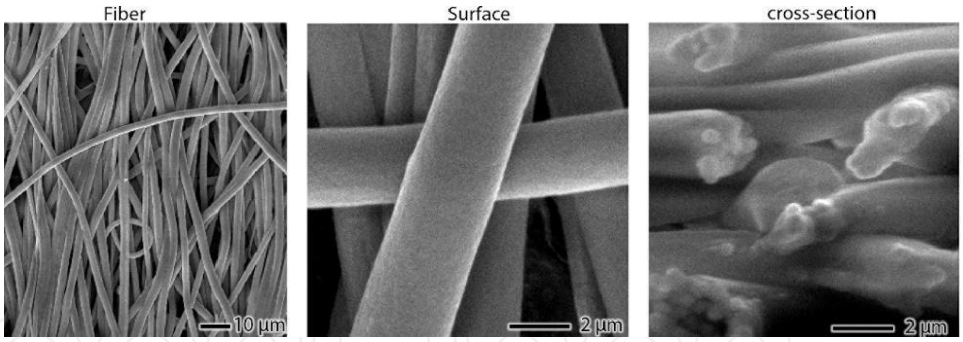

Figure 3. SEM images of the overview, surface, and cross-section of LAPS nanofibers prepared by thermally triggered encapsulation at 50 °C [29].

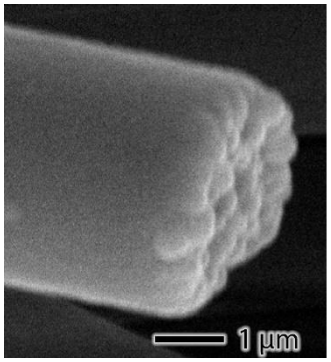

Figure 4. SEM image showing the cross-section of LAPS prepared by solvent-assisted encapsulation using 0.4 g/ml LA ethanol solution [30].

surface tension effects. The accumulation of FA eutectics supported on or near the surface resulted in an unclear distinction between PCM and polymer framework. However, the overall shape of the nanofibers was retained and prevented leakage to some extent [32, 64].

Coaxial electrospun PCM composite nanofibers are able to fully encapsulate PCM in the interior core by trapping with a continuous outer sheath layer of polymer, providing mechanical support and containment. SEM images of nanofibers with PEG core and CA sheath show cylindrical and smooth fiber surfaces before and after thermal cycling. The diameter of the fibers increased with increasing PEG loading. The structure of CA nanofibers after the removal of PEG indicated the uniform distribution and complete encapsulation of the PCM and continuous and uniform CA sheath [25]. Coaxial electrospun octadecane/PVB nanofibers demonstrated that the electrospinning process was negatively impacted when the polymer concentration was not ideal. In nanofibers produced from sheath solutions with low

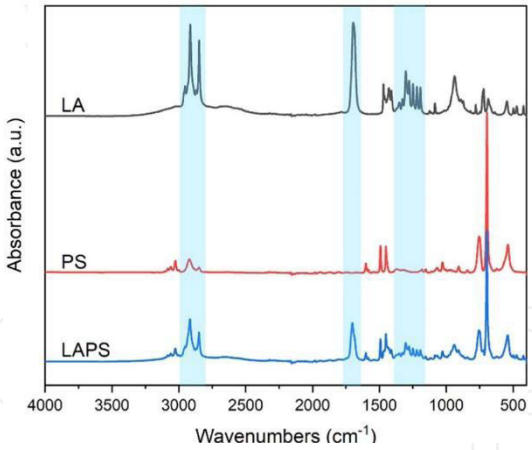

Figure 5. ATR spectra of LA, PS, and LAPS composite nanofibers prepared from 0.4 g/ml LA ethanol solution and 1 h encapsulation time [30].

PVB concentration, swollen and broken fibers were observed since the PVB was not able to completely encapsulate octadecane. At a higher PVB concentration, the nanofibers were unbroken and the PVB sheath completely encapsulated octadecane. This was confirmed by a petroleum ether wash that exposed a dense shell and a hollow core structure [51].

Uniaxial blend electrospun nanofibers do not possess the sheath outer layer. SEM images of uniaxial blend electrospun nanofibers of plant wax mixture/PVA show rough and uniform surface. The roughness increased with increasing PCM content. At high PCM concentrations, thinner fibers and occasional clusters were observed. The incorporation of PCM in the PVA nanofibers increased the average fiber diameter from 228.18 nm to 634.66 nm in 7% PVA and from 360.63 nm to 760.18 nm in 9% PVA [21]. Blend electrospun LAPA6 composite nanofibers displayed rough surface and ribbon shape. The LAPA6 nanofibers with smooth surface and uniform cylindrical shape had larger diameters than the pure PA6 nanofibers [66].

3.3. Chemical structure

The entrapment of PCMs in composite materials such as nanofiber membranes can be confirmed by using Infrared spectroscopy (IR) and Raman spectroscopy. Successful entrapment of PCMs inside a material can be confirmed by examining the material's interior and surface properties. The IR signals corresponding to LA are 2915 cm^{-1} (CH_3), 2848 cm^{-1} (CH_2), 1695 cm^{-1} (C = O), 1470–1410 cm^{-1} (CH_3 and CH_2), and 1085 cm^{-1} (C–O) as well as others. The IR signals corresponding to PS are 3029 cm^{-1} (aromatic CH), 2923 cm^{-1} (aliphatic CH_2 and CH), 1493 and 1452 cm^{-1} (aromatic CC). A strong and unique carbonyl peak at 1695 cm^{-1} can be used as an indicator of LA content. IR spectra of the blend electrospun LAPS composite

nanofibers showed an increasing signal for the peak at 1695 cm^{-1} with increasing LA content. Raman spectroscopy is a scattering technique and as such can only analyze the surface of the material. The Raman spectra lacked LA peaks and therefore confirmed no surface LA [28]. The IR spectra of LAPS nanofibers prepared by thermally triggered encapsulation, shown in figure 5, had a slightly weakened LA carbonyl peak when the temperature was increased from 50 °C to 60 °C, and the carbonyl peak almost disappeared in samples prepared at 70 °C and 80 °C. The Raman spectra signal for LA also decreased. This suggested that the amount of LA decreased at higher temperatures and agreed with SEM observations [29]. The Raman spectra of LAPS composite fibers prepared by solvent-assisted encapsulation showed flattened peaks of those observed for pristine LA (1500–900 cm^{-1}). This confirmed successful encapsulation of LA in nanofibers, which agreed with the SEM observations [30].

3.4. PCM stability during phase change

The widespread implementation of PCMs for TES systems is limited due to the lack of sufficiently long-term stability of storage materials [15]. A reliable TES system requires thermal, chemical, and physical stability after repeated thermal cycles. The thermo-physical properties of PCM composite nanofibers for TES systems are typically not largely altered by thermal cycles and thus are relatively thermally stable and have long life spans [67]. The long-term thermal stability of TES systems is analyzed by investigating the thermo-physical properties after going through thermal cycles repeatably. Accelerated thermal cycle tests using an oven or temperature controlled electric hot plate can be used to simulate the thermal cycles of a TES system. A small sample can be used to test the thermo-physical properties after a number of cycles. Thermal stability of latent heat storage is indicated by negligible change of melting point and enthalpy of fusion [65]. The TGA-DSC thermogram of blend electrospun LAPS nanofibers showed that onset temperature of PS degradation was unaffected and demonstrated that the integrity of PS was unaffected by LA content. The containment of a liquid PCM after phase change requires continuous and uniform polymer supporting material. This was tested in the LAPS composite nanofibers by removing LA using ethanol, a solvent for LA and nonsolvent for PS. IR spectra as well as TGA-DSC suggested the complete removal of LA. The PS nanofibers were examined again by SEM and found to be continuous without any breaks or cavities. Additionally, the PS nanofibers were highly porous after the removal of LA. Thermal-induced leakage of LA was investigated by heating to 60 °C for 24 h. The heat-treated LAPS nanofibers had a strong absorbance at 1695 cm^{-1}, corresponding to LA. Slight curling of the membrane edges, common for thermal sensitive membranes, was observed but no LA droplets were found on the

underlying aluminum foil. TGA-DSC analysis closely matched the weight loss and LA content of the original LAPS composite nanofibers, indicating proper PCM containment without noticeable PCM leakage [28].

The stability of LAPS nanofibers prepared by thermally triggered encapsulation was examined by 100 continuous heating-cooling cycles using DSC, as shown in figure 6. The melting and crystallization temperatures slightly shifted and the shape of melting thermograms was retained. The heat flow during crystallization was altered after 100 thermal cycles and in the case of the $LAPS_{50}$, the peak split from a single to double peaks. This was likely a result of the formation of tiny channels connecting the internal LA to the surface of the nanofibers during the thermal expansion and contraction of PS and melting and crystallization of LA. However, variations in the overall heat released during crystallization were negligible. The enthalpy of crystallization was found to be 146.7 J/g for the 1st cycle and 146.4 J/g after the 100th cycle for $LAPS_{50}$ composite nanofibers. The LAPS nanofibers demonstrated a robust thermal cycling stability and reusability with retained thermal energy storage capability without notable deterioration [29]. The stability of LAPS composite nanofibers prepared by solvent-assisted encapsulation was examined by 100 continuous heating-cooling cycles by DSC. SEM images after 100 thermal cycles confirmed the successful encapsulation of LA by a lack of any observable leakage, no LA droplets on surface or interfiber spacing, and densely packed LA domains in the interior. The removal of LA by ethanol resulted in PS nanofibers displaying porous interiors but no breaks [30]. The thermal stability of fatty acid eutectic/SiO_2 composite nanofibers were examined by 50 DSC thermal cycles. The thermogram did not show any notable change in enthalpy of crystallization and good thermal reliability, suggesting a long lifetime of use [64]. However, the lower number of thermal cycles and lack of additional methods of testing the PCM composite nanofibers alludes to the questionable thermal stability of these form-stable PCM nanofiber membranes.

Coaxial electrospun PCM composite nanofibers demonstrated good thermal stability during phase change. This was demonstrated by 100 thermal cycles in DSC for PEG core-CA sheath nanofibers. The enthalpies of crystallization only decreased by 0.5–0.7 J/g [25]. The thermal stability of octadecane/PVB core-sheath nanofibers was investigated by periodic simulated solar irradiation of model houses during repeated heating/cooling cycles. The inner temperatures of the model houses showed good repeatability. These results indicated the complete encapsulation, stability, and reliability of the PCM composite material [51].

Uniaxial electrospun PCM composite nanofibers also demonstrated less desirable thermal stability during phase change. The thermal stability of uniaxial blend electrospun mixture of plant oils and PVA was investigated by DCS thermal cycling for 10 cycles and heat treatment in a convection oven at 50–80 °C for 5 min to 2 h.

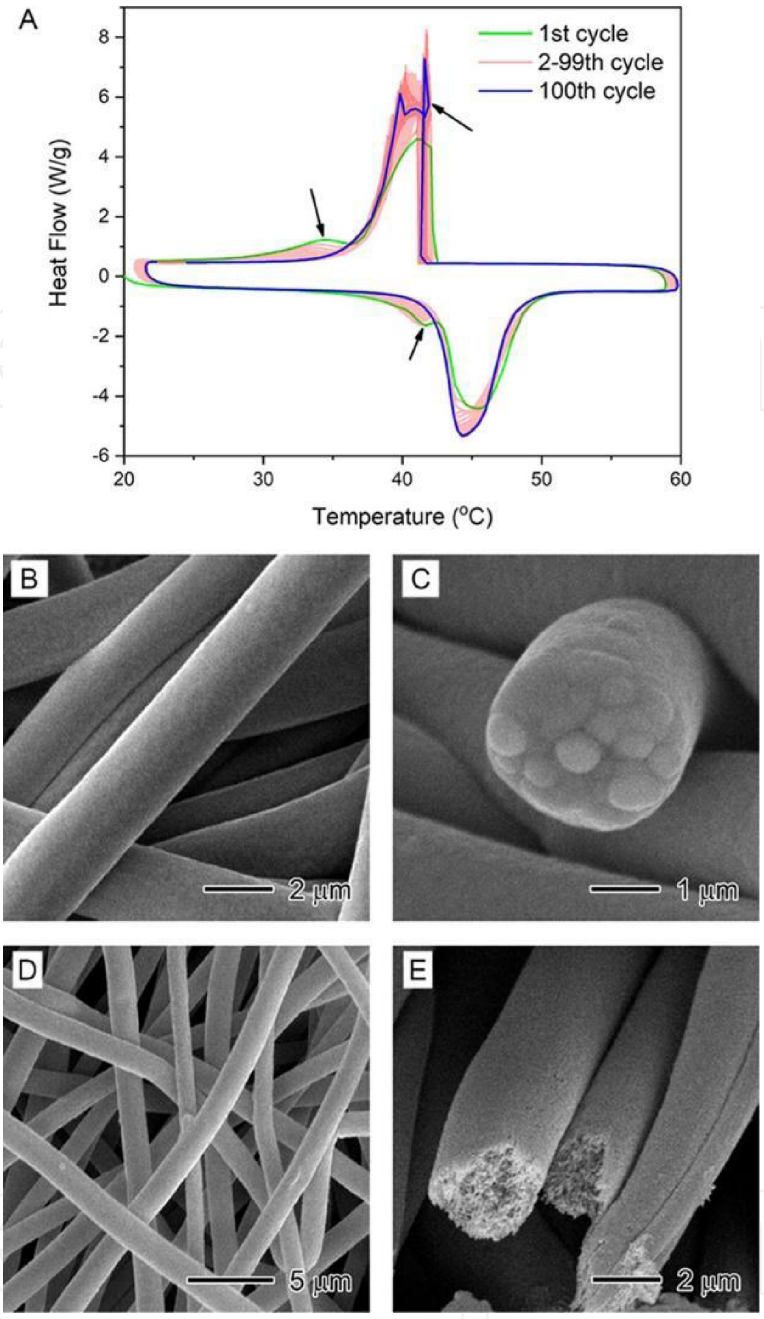

Figure 6. 100 thermal cycle (20–60 °C) DSC thermogram of LAPS composite nanofibers prepared with 0.4 g/ml LA ethanol solution and 1 h encapsulation time (A), LAPS nanofibers after 100 thermal cycles (B,C), and LAPS nanofibers after 100 thermal cycles and LA removal by ethanol (D,E) [30].

The maximum enthalpy of melting decreased by 0.31 J/g after 10 thermal cycles. For the nanofibers electrospun from a lower PVA concentration, after 2 h at 50–60 °C, surface porosity was retained; however, at 70–80 °C smooth surfaces were observed,

indicating PCM distribution across the surface. The higher PVA concentration composite nanofibers showed an increase in number of pores after thermal treatment, indicating PCM leakage. The difference in polarity between the PCM and PVA caused phase separation during PCM melting and PCM was observed to accumulate on the fiber surface or interfiber spacing [21].

4. Conclusions

Thermal energy storage of latent heat by PCM composite materials is a promising approach for improving thermal management and efficiency of energy storage and use. Typical core-shell PCM capsules have limited loading capacity and PCM content is further reduced after incorporating into bulk material. Electrospun nanofibers have gained considerable attention recently as a facile approach for the fabrication of continuous nonwoven nano- and micro-meter scale fibers from a wide range of materials and composites. The properties of nanofibers are enhanced by their small size and extremely large specific surface area. This imparts faster retrieval and release of thermal energy. Blend and coaxial electrospinning techniques have been extensively researched for the manufacturing of PCM composite nanofibers. These traditional electrospinning techniques have limitations on maximum PCM content, distribution, and thermal energy storage capacity. The LAPS composite nanofibers produced by blend electrospinning and post electrospinning encapsulation techniques showed high PCM loading and thermal energy storage capacity. The LAPS nanofibers prepared by solvent-assisted encapsulation had the highest loading of PCM and thermal energy storage capacity of 82.0% and 147.8 J/g, respectively. The incorporation of LA in PS nanofibers was examined by SEM imaging and complete encapsulation was confirmed by IR and Raman. The post electrospinning encapsulation technique had similarly high PCM loading as PCM absorption technique, but with the added benefits of complete internal encapsulation of PCM, no interfiber membrane PCM containment, and higher thermal energy storage capacity. The stability of LAPS nanofibers prepared by solvent-assisted encapsulation was confirmed by 100 thermal cycles using DSC. This PCM composite nanofiber preparation technique proved to be highly efficient in PCM encapsulation and thermal energy storage capacity as well as highly stable in thermal cycles.

Data availability

The data presented in this study are available on request from the corresponding author.

Conflict of interest

The authors declare no conflict of interest.

References

1 **Reneker D. H.**, **Yarin A. L.** Electrospinning jets and polymer nanofibers. ***Polymer***, 2008; **49**(10): 2387–2425. doi:10.1016/j.polymer.2008.02.002.

2 **Taylor G.** Disintegration of water drops in an electric field. ***Proc. R. Soc. Lond. Math. Phys. Sci.***, 1964; **280**(1382): 383–397.

3 **Wendorff J. H.**, **Agarwal S.**, **Greiner A.**, **Agarwal a. S.** Electrospinning : Materials, Processing, and Applications. Hoboken, NJ: John Wiley & Sons, Incorporated, 2012.

4 **Wang J.**, **Yao S.**, **Ma Y.**, **Liu W.** Electrode polarity effects in electrospinning organic/inorganic hybrid nanofibers. ***Ceram. Int.***, 2021; **47**(3): 4352–4356. doi:10.1016/j.ceramint.2020.09.285.

5 **Kayaci F.**, **Ozgit-Akgun C.**, **Donmez I.**, **Biyikli N.**, **Uyar T.** Polymer-inorganic core-shell nanofibers by electrospinning and atomic layer deposition: flexible nylon-ZnO core-shell nanofiber mats and their photocatalytic activity. ***ACS Appl. Mater. Interfaces***, 2012; **4**(11): 6185–6194. doi:10.1021/am3017976.

6 **Ramakrishna S.**, **Fujihara K.**, **Teo W.-E.**, **Lim T.-C.**, **Ma Z.** An Introduction to Electrospinning and Nanofibers. Singapore: World Scientific Publishing Co., 2005.

7 **Mercante L. A.**, **Scagion V. P.**, **Migliorini F. L.**, **Mattoso L. H .C.**, **Correa D. S.** Electrospinning-based (bio)sensors for food and agricultural applications: A review. ***TrAC Trends Anal. Chem.***, 2017; **91**: 91–103. doi:10.1016/j.trac.2017.04.004.

8 **Luraghi A.**, **Peri F.**, **Moroni L.** Electrospinning for drug delivery applications: A review. ***J. Control Release***, 2021; **334**: 463–484. doi:10.1016/j.jconrel.2021.03.033.

9 Filtering Media by Electrospinning Next Generation Membranes for Separation Applications. In: Focarete M. L., Gualandi C., Ramakrishna S. (eds), Swiss: Springer International Publishing AG, 2018. doi:10.1007/978-3-319-78163-1.

10 Electrospun Nanofibers for Energy and Environmental Applications.. In: Lockwood D. J. (ed.), Berlin, Heidelberg: Springer-Verlag, 2014doi:10.1007/978-3-642-54160-5.

11 **Safari A.**, **Saidur R.**, **Sulaiman F. A.**, **Xu Y.**, **Dong J.** A review on supercooling of phase change materials in thermal energy storage systems. ***Renew. Sustain. Energy Rev.***, 2017; **70**: 905–919. doi:10.1016/j.rser.2016.11.272.

12 **Pielichowska K.**, **Pielichowski K.** Phase change materials for thermal energy storage. ***Prog. Mater. Sci.***, 2014; **65**: 67–123. doi:10.1016/j.pmatsci.2014.03.005.

13 **l-Dessouky H.**, **l-Juwayhel F.** Effectiveness of a thermal energy storage system using phase-change materials. ***Energy Convers. Manag.***, 1997; **38**(6): 601–617. doi:10.1016/S0196-8904(96)00072-6.

14 **Kenisarin M.**, **Mahkamov K.** Solar energy storage using phase change materials. ***Renew. Sustain. Energy Rev.***, 2007; **11**(9): 1913–1965. doi:10.1016/j.rser.2006.05.005.

15 **Sharma A.**, **Tyagi V. V.**, **Chen C. R.**, **Buddhi D.** Review on thermal energy storage with phase change materials and applications. ***Renew. Sustain. Energy Rev.***, 2009; **13**(2): 318–345. doi:10.1016/j.rser.2007.10.005.

16 **Sarier N.**, **Onder E.** Organic phase change materials and their textile applications: an overview. ***Thermochim Acta***, 2012; **540**: 7–60. doi:10.1016/j.tca.2012.04.013.

17 **Prajapati D. G.**, **Kandasubramanian B.** Biodegradable polymeric solid framework-based organic phase-change materials for thermal energy storage. ***Ind. Eng. Chem. Res.***, 2019; **58**(25): 10652–10677. doi:10.1021/acs.iecr.9b01693.

18 **Wu Y.**, **Chen C.**, **Jia Y.**, **Wu J.**, **Huang Y.**, **Wang L.** Review on electrospun ultrafine phase change fibers (PCFs) for thermal energy storage. ***Appl. Energy***, 2018; **210**: 167–181.

19 **Zhao L.**, **Luo J.**, **Li Y.**, **Wang H.**, **Song G.**, **Tang G.** Emulsion-electrospinning n-octadecane/silk composite fiber as environmental-friendly form-stable phase change materials. ***J. Appl. Polym. Sci.***, 2015; **134**: 45538. doi:10.1002/APP.45538.

20 **Perez-Masia R.**, **Lopez-Rubio A.**, **Fabra M. J.**, **Lagaron J. M.** Biodegradable polyester-based heat management materials of interest in refrigeration and smart packaging coatings. ***J. Appl. Polym. Sci.***, 2013; **130**(5): 3251–3262. doi:10.1002/app.39555.

21 **Zdraveva E.**, **Fang J.**, **Mijovic B.**, **Lin T.** Electrospun poly(vinyl alcohol)/phase change material fibers: morphology, heat properties, and stability. ***Ind. Eng. Chem. Res.***, 2015; **54**: 8706–8712. doi:10.1021/acs.iecr.5b01822.

22 **Hu W.**, **Yu X.** Thermal and mechanical properties of bio-based PCMs encapsulated with nanofibrous structure. ***Renew. Energy***, 2014; **62**: 454–458.

23 **Rezaei B.**, **Ghani M.**, **Askari M.**, **Shoushtari A. M.**, **Malek R. M. A.** Fabrication of thermal intelligent core/shell nanofibers by the solution coaxial electrospinning process. ***Adv. Polym. Technol.***, 2016; **35**(1): 21534. doi:10.1002/adv.21534.

24 **Do C. V.**, **Nguyen T. T. T.**, **Park J. S.** Fabrication of polyethylene glycol/polyvinylidene fluoride core/shell nanofibers via melt electrospinning and their characteristics. ***Sol. Energy Mater. Sol. Cells***, 2012; **104**: 131–139.

25 **Chen C.**, **Zhao Y.**, **Liu W.** Electrospun polyethylene glycol/cellulose acetate phase change fibers with coreesheath structure for thermal energy storage. ***Renew. Energy***, 2013; **60**: 222–225.

26 **Noyan E. C. B.**, **Onder E.**, **Sarier N.**, **Arat R.** Development of heat storing poly(acrylonitrile) nanofibers by coaxial electrospinning. ***Thermochim Acta***, 2018; **662**: 135–148. doi:10.1016/j.tca.2018.02.008.

27 **Seifpoor M.**, **Nouri M.**, **Mokhtari J.** Thermo-regulating nanofibers based on nylon 6,6/polyethylene glycol blend. ***Fibers Polym.***, 2010; **12**(6): 706–714. doi:10.1007/s12221-011-0706-z.

28 **Lu P.**, **Chen W.**, **Zhu M.**, **Murray S.** Embedding lauric acid into polystyrene nanofibers to make high-capacity membranes for efficient thermal energy storage. ***ACS Sustain. Chem. Eng.***, 2017; **5**(8): 7249–7259. doi:10.1021/acssuschemeng.7b01476.

29 **Lu P.**, **Chen W.**, **Fan J.**, **Ghaban R.**, **Zhu M.** Thermally triggered nanocapillary encapsulation of lauric acid in polystyrene hollow fibers for efficient thermal energy storage. ***ACS Sustain. Chem. Eng.***, 2018; **6**(2): 2656–2666. doi:10.1021/acssuschemeng.7b04259.

30 **Ghaban R.**, **Duong J.**, **Patel D.**, **Singh H.**, **Chen W.**, **Lu P.** Solvent-assisted nanochannel encapsulation of a natural phase change material in polystyrene hollow fibers for high-performance thermal energy storage. ***ACS Appl. Energy Mater.***, 2020; **3**(10): 10089–10096. doi:10.1021/acsaem.0c01788.

31 **Zong X.**, **Cai Y.**, **Sun G.**, **Zhao Y.**, **Huang F.**, **Song L. et al.** Fabrication and characterization of electrospun SiO_2 nanofibers absorbed with fatty acid eutectics for thermal energy storage/retrieval. ***Sol. Energy Mater. Sol. Cells***, 2015; **132**: 183–190.

32 **Cai Y.**, **Xu X.**, **Gao C.**, **Bian T.**, **Qiao H.**, **Wei Q.** Structural morphology and thermal performance of composite phase change materials consisting of capric acid series fatty acid eutectics and electrospun polyamide6 nanofibers for thermal energy storage. ***Mater. Lett.***, 2012; **89**: 43–46.

33 **Cai Y.**, **Ke H.**, **Lin L.**, **Fei X.**, **Wei Q.**, **Song L. et al.** Preparation, morphology and thermal properties of electrospun fatty acid eutectics/polyethylene terephthalate form-stable phase change ultrafine composite fibers for thermal energy storage. ***Energy Convers. Manag.***, 2012; **64**: 245–255. doi:10.1016/j.enconman.2012.04.018.

34 **Jamekhorshid A.**, **Sadrameli S. M.**, **Farid M.** A review of microencapsulation methods of phase change materials (PCMs) as a thermal energy storage (TES) medium. ***Renew. Sustain. Energy Rev.***, 2014; **31**: 531–542. doi:10.1016/j.rser.2013.12.033.

35 **Fei B.**, **Lu H.**, **Qi K.**, **Shi H.**, **Liu T.**, **Li X. et al.** Multi-functional microcapsules produced by aerosol reaction. ***J. Aerosol Sci.***, 2008; **39**(12): 1089–1098. doi:10.1016/j.jaerosci.2008.07.007.

36 **Borreguero A. M.**, **Valverde J. L.**, **Rodríguez J. F.**, **Barber A. H.**, **Cubillo J. J.**, **Carmona M.** Synthesis and characterization of microencapsules containing Rubitherm RT27 obtained by spray drying. ***Chem. Eng. J.***, 2011; **166**(1): 384–390. doi:10.1016/j.cej.2010.10.055.

37 **iChen Z.**, **Cao L.**, **Shan F.**, **Fang G.** Preparation and characteristics of microencapsulated stearic acid as composite thermal energy storage material in buildings. ***Energy Build.***, 2013; **62**: 469–474. doi:10.1016/j.enbuild.2013.03.025.

38 **Ghosh S. K.** Functional Coatings: By Polymer Microencapsulation. Germany: Wiley-VCH, 2006.

39 **Liang S.**, **Zhu Y.**, **Wang H.**, **Wu T.**, **Tian C.**, **Wang J. et al.** Preparation and characterization of thermoregulated rigid polyurethane foams containing nanoencapsulated phase change materials. ***Ind. Eng. Chem. Res.***, 2016; **55**(10): 2721–2730. doi:10.1021/acs.iecr.5b04543.

40 **You M.**, **Zhang X. X.**, **Li W.**, **Wang X. C.** Effects of MicroPCMs on the fabrication of MicroPCMs/polyurethane composite foams. ***Thermochim. Acta***, 2008; **472**(1–2): 20–24. doi:10.1016/j.tca.2008.03.006.

41 **Cheng P.**, **Wei K.**, **Shi W.**, **Shi J.**, **Wang S.**, **Ma B.** Preparation and performance analysis of phase change microcapsule/epoxy resin composite phase change material. ***J. Energy Storage***, 2022; **47**: 103581. doi:10.1016/j.est.2021.103581.

42 **Li W.**, **Ma Y.-j.**, **Tang X.-f.**, **Jiang N.**, **Zhang R.**, **Han N. et al.** Composition and characterization of thermoregulated fiber containing acrylic-based copolymer microencapsulated phase-change materials (MicroPCMs). ***Ind. Eng. Chem. Res.***, 2014; **53**(13): 5413–5420. doi:10.1021/ie4041174a.

43 **Schmidt M.**, **Kusche R.**, **Issendorff B. v.**, **Haberland H.** Irregular variations in the melting point of size-selected atomic clusters. ***Lett. Nat.***, 1998; **393**: 238–240.

44 **Chalco-Sandoval W.**, **Fabra M. J.**, **López-Rubio A.**, **M.Lagaron J.** Use of phase change materials to develop electrospun coatings of interest in food packaging applications. ***J. Food Eng.***, 2017; **192**: 122–128. doi:10.1016/j.jfoodeng.2015.01.019.

45 Morphology and performances of electrospun polyethylene glycol/poly (dl-lactide) phase change ultrafine fibers for thermal energy storage. ***Sol. Energy Mater. Sol. Cells***, 2013; **117**: 372–381. doi:10.1016/j.solmat.2013.07.001.

46 **Sarier N.**, **Arat R.**, **Menceloglu Y.**, **Onder E.**, **Boz E. C.**, **Oguz O.** Production of PEG grafted PAN copolymers and their electrospun nanowebs as novel thermal energy storage materials. ***Thermochim. Acta***, 2016; **643**: 83–93. doi:10.1016/j.tca.2016.10.002.

47 **McCann J. T.**, **Marquez M.**, **Xia Y.** Melt coaxial electrospinning: a versatile method for the encapsulation of solid materials and fabrication of phase change nanofibers. ***Nano Lett.***, 2006; **6**(12): 2868–2872. doi:10.1021/nl0620839.

48 **Hu W.**, **Yu X.** Encapsulation of bio-based PCM with coaxial electrospun ultrafine fibers. ***RSC Adv.***, 2012; **2**: 5580–5584. doi:10.1039/c2ra20532g.

49 **Feng W.**, **Zhang Y.-s.**, **Shao Y.-w.**, **Huang T.**, **Zhang N.**, **Yang J.-h. et al.** Coaxial electrospun membranes with thermal energy storage and shape memory functions for simultaneous thermal/moisture management in personal cooling textiles. ***Eur. Polym. J.***, 2021; **145**: 110245. doi:10.1016/j.eurpolymj.2020.110245.

50 **Dang T. T.**, **Nguyen T. T. T.**, **Chung O. H.**, **Park J. S.** Fabrication of form-stable poly(ethylene glycol)-loaded poly(vinylidene fluoride) nanofibers via single and coaxial electrospinning. ***Macromol. Res.***, 2015; **23**: 819–829. doi:10.1007/s13233-015-3109-y.

51 **Sun S.-X.**, **Xie R.**, **Wang X.-X.**, **Wen G.-Q.**, **Liu Z.**, **Wang W. et al.** Fabrication of nanofibers with phase-change core and hydrophobic shell, via coaxial electrospinning using nontoxic solvent. ***J. Mater. Sci.***, 2015; **50**: 5729–5738. doi:10.1007/s10853-015-9118-6.

52 **Chen C.**, **Zhao Y.**, **Liu W.** Electrospun polyethylene glycol/cellulose acetate phase change fibers with core-sheath structure for thermal energy storage. ***Renew. Energy***, 2013; **60**: 222–225. doi:10.1016/j.renene.2013.05.020.

53 **Zamani M.**, **Prabhakaran M. P.**, **Ramakrishna S.** Advancements in drug delivery via electrospun and electrosprayed nanomaterials. ***Int. J. Nanomed.***, 2013; **8**: 2997–3017. doi:10.2147/IJN.S43575.

54 **Kizildag N.** Smart composite nanofiber mats with thermal management functionality. ***Sci. Rep.***, 2021; **11**: 4256. doi:10.1038/s41598-021-83799-5.

55 **Lu P.**, **Xia Y.** Maneuvering the internal porosity and surface morphology of electrospun polystyrene yarns by controlling solvent and relative humidity. ***Langmuir***, 2013; **29**: 7070–7078.

56 **Tang X.**, **Li W.**, **Shi H.**, **Wang X.**, **Wang J.**, **Zhang X.** Fabrication, characterization, and supercooling suppression of nanoencapsulated n-octadecane with methyl methacrylate–octadecyl methacrylate copolymer shell. ***Colloid Polym. Sci.***, 2013; **291**: 1705–1712. doi:10.1007/s00396-013-2905-1.

57 **Chen C.**, **Wang L.**, **Huang Y.** Electrospun phase change fibers based on polyethylene glycol/cellulose acetate blends. ***Appl. Energy***, 2011; **88**: 3133–3139. doi:10.1016/j.apenergy.2011.02.026.

58 **Rathore P.**, **Schiffman J. D.** Beyond the single-nozzle: coaxial electrospinning enables innovative nanofiber chemistries, geometries, and applications. ***ACS Appl. Mater. Interfaces***, 2021; **13**: 48–66. doi:10.1021/acsami.0c17706.

59 **Nguyen T. T. T.**, **Ghosh C.**, **Hwang S.-G.**, **Chanunpanich N.**, **Park J. S.** Porous core/sheath composite nanofibers fabricated by coaxial electrospinning as a potential mat for drug release system. ***Int. J. Pharm.***, 2012; **439**(1–2): 296–306.

60 **Lu Y.**, **Xiao X.**, **Fu J.**, **Huan C.**, **Qi S.**, **Zhan Y. et al.** Novel smart textile with phase change materials encapsulated core-sheath structure fabricated by coaxial electrospinning. ***Chem. Eng. J.***, 2019; **355**: 532–539.

61 **Yang X.**, **Yuan Y.**, **Zhang N.**, **Cao X.**, **Liu C.** Preparation and properties of myristic-palmitic-stearic acid/expanded graphite composites as phase change materials for energy storage. ***Sol. Energy***, 2014; **99**: 259–266. doi:10.1016/j.solener.2013.11.021.

62 **Zhang N.**, **Yuan Y.**, **Wang X.**, **Cao X.**, **Yang X.**, **Hu S.** Preparation and characterization of lauric-myristic-palmitic acid ternary eutectic mixtures/expanded graphite composite phase change material for thermal energy storage. ***Chem. Eng. J.***, 2013; **231**: 214–219. doi:10.1016/j.cej.2013.07.008.

63 **Brown H. R.** The theory of the rise of sap in trees: some historical and conceptual remarks. ***Phys. Perspect.***, 2013; **15**(3): 320–358. doi:10.1007/s00016-013-0117-1.

64 **Cai Y.**, **Sun G.**, **Liu M.**, **Zhang J.**, **Wang Q.**, **Wei Q.** Fabrication and characterization of capric–lauric–palmitic acid/electrospun SiO_2 nanofibers composite, structural morphology and thermal performance of composite phase change material. ***Solar Energy***, 2015; **118**: 87–95. doi:10.1016/j.solener.2015.04.042.

65 **Rathod M. K.**, **Banerjee J.** Thermal stability of phase change materials used in latent heat energy storage systems: a review. ***Renew. Sustain. Energy Rev.***, 2013; **18**: 246–258. doi:10.1016/j.rser.2012.10.022.

66 **Cai Y.**, **Gao C.**, **Xu X.**, **Fu Z.**, **Fei X.**, **Zhao Y. et al.** Electrospun ultrafine composite fibers consisting of lauric acid and polyamide 6 as form-stable phase change materials for storage and retrieval of solar thermal energy. ***Sol. Energy Mater. Sol. Cells***, 2012; **103**: 53–61. doi:10.1016/j.solmat.2012.04.031.

67 **Huang X.**, **Alva G.**, **Jia Y.**, **Fang G.** Morphological characterization and applications of phase change materials in thermal energy storage: a review. ***Renew. Sustain. Energy Rev.***, 2017; **72**: 128–145. doi:10.1016/j.rser.2017.01.048.